| | |
|---|---|
| Title | Hybrid structure of cobalt monoxide nanowire @ nickel hydroxidenitrate nanoflake aligned on nickel foam for high-rate supercapacitor |
| Author(s) | Guan, Cao; Liu, Jinping; Cheng, Chuanwei; Li, Hongxing; Li, Xianglin; Zhou, Weiwei; Zhang, Hua; Fan, Hong Jin |
| Citation | Guan, C., Liu, J., Cheng, C., Li, H., Li, X., Zhou, W., et al. (2011). Hybrid structure of cobalt monoxide nanowire @ nickel hydroxidenitrate nanoflake aligned on nickel foam for high-rate supercapacitor. Energy & Environmental Science, 4(11), 4496-4499. |
| Date | 2011 |
| URL | http://hdl.handle.net/10220/8362 |
| Rights | © 2011 The Royal Society of Chemistry. This is the author created version of a work that has been peer reviewed and accepted for publication by Energy & Environmental Science, The Royal Society of Chemistry. It incorporates referee's comments but changes resulting from the publishing process, such as copyediting, structural formatting, may not be reflected in this document. The published version is available at: http://dx.doi.org/10.1039/c1ee01685g. |

Energy &
Environmental Science

Dynamic Article Links

Cite this: DOI: 10.1039/c0xx00000x

www.rsc.org/xxxxxx

ARTICLE TYPE

# Hybrid structure of cobalt monoxide nanowire @ nickel hydroxidenitrate nanoflake aligned on nickel foam for high-rate supercapacitor†‡

**Cao Guan,[ac] Jinping Liu,[a] Chuanwei Cheng,[a] Hongxing Li,[a] Xianglin Li,[a] Weiwei Zhou,[a] Hua Zhang[b] and Hong Jin Fan*[ac]**

*Received (in XXX, XXX) Xth XXXXXXXXX 20XX, Accepted Xth XXXXXXXXX 20XX*
**DOI: 10.1039/b000000x**

**A new hybrid nanostructure of porous cobalt monoxide nanowire @ ultrathin nickel hydroxidenitrate nanoflake is directly synthesized on a 3D nickel foam by a facile two-step hydrothermal route, which demonstrates a specific capacitance of ~798.3 F $g^{-1}$ at the current density of ~1.67 A $g^{-1}$ and good rate performance when used as electrode material for supercapacitors. The capacitance loss is less than 5% after 2000 charge–discharge cycles.**

Supercapacitors are playing an important role in hybrid electric vehicles and industrial equipments.[1,2] Consumer demand is driving research efforts for novel electrode materials with higher energy storage capability, better rate property and cycling stability. Among the numerous materials studied so far, transition metal (Mn, Fe, Co, Ni, Ru, *etc.*) oxides and hydroxides are good candidates for supercapacitors because of their variety of oxidation states for charge transfer and high mass densities. Nanotechnology can enhance their redox kinetics which are usually limited by the physical changes during charge/discharge (caused by ion diffusion and electron transfer), so fabricating nanosized transition metal oxides and hydroxides is a good way to achieve high specific capacities (SCs) in experiments.[3–8] Ruthenium oxide nanotubes have shown a capacitance as high as 1300 F $g^{-1}$ in an aqueous acidic electrolyte.[9] Unfortunately, the expensive nature and toxicity of ruthenium has limited it from extensive commercialization. Other cost-effective and nontoxic nanomaterials of $MnO_2$,[10] $Co_3O_4$,[11,12] and $Fe_3O_4$,[13] when served as active materials, have also demonstrated improved performance over bulk materials. Further efforts have been devoted to compound these metal oxides and hydroxides with conductive metals,[14] graphitic supports,[15–17] or conducting polymers.[18] Although better properties have been achieved, the reaction was typically at a low charge/discharge rate, and the content of these active materials for supercapacitors was relatively scarce, therefore energy and power per unit area were to some extent low. Mixed metal oxides[19] were tested recently, but their electrochemical performance was far from satisfactory, partially because of the lack of well-defined micro-/nanostructure. Three-dimensional (3D) hybrid nanostructure, with short ion diffusion path and enlarged surface area, provides more efficient contact between electrolyte ion and active materials for Faradaic energy storage,[20] thus it is a promising way to build better electrochemical materials. For example, 3D hybrid nanostructures of $Zn_2SnO_4$ @ $MnO_2$[21] and ZnO @ $MoO_3$[22] have significantly enhanced both the capacitance and durability of supercapacitors.

Herein, we report a novel 3D hybrid structure of porous cobalt monoxide (CoO) nanowire @ ultrathin nickel hydroxidenitrate (NiHON) nanoflake directly grown on nickel foam, which has robust hierarchical porosity and high specific surface area. One significant difference of this structure from precious mentioned 3D hybrid

[a]*Division of Physics and Applied Physics, School of Physical and Mathematical Sciences, Nanyang Technological University, 21 Nanyang Link, 637371, Singapore. E-mail: fanhj@ntu.edu.sg*
[b]*School of Materials Science and Engineering, Nanyang Technological University, 639798, Singapore*
[c]*Energy Research Institute @ NTU (ERIAN), 50 Nanyang Drive, 637553, Singapore*

† Electronic supplementary information (ESI) available: CV and charge–discharge testing of nickel foam, NiHON powder sample testing and specific capacitance calculation. See DOI: 10.1039/c1ee01685g

‡ This article was submitted following the ICCES Clean Energy conference in Dalian, China.

## Broader context

Supercapacitors are a promising candidate for next-generation energy storage devices as they have large specific capacitance, long cycling life, and can provide a much higher power density than conventional batteries. The key task is to build high-performance electrode materials. In this communication, a new integrated hybrid structure with two active nanomaterials is fabricated on a three-dimensional (3D) nickel foam substrate. CoO nanowires serve as conductive backbones and the ultrathin nickel-based nanoflakes further enlarge the contact area with electrolyte. When tested as a supercapacitor anode, this hybrid structure exhibits an excellent electrochemical stability, good rate performance and a maximum specific capacitance of (798.3 F $g^{-1}$), as a result of a synergic effect of both active materials as well as the nickel foam.

nanostructures is that both CoO and NiHON are employed as active electrode materials on account that they both have relatively high capacitance.[23,24] Besides, CoO with well-defined single-crystalline nanostructure serves as both the backbone and conductive connection for NiHON, and its porous feature can enlarge the specific surface area. Ultrathin nanoflake-like NiHON can enlarge the contact area with electrolyte, enable fast redox reaction, and protect the inner structure of CoO thus improve the durability. In our work, nickel foam was selected as a cost-effective substrate because of its high conductivity and 3D network structure, so it can: (1) reduce the diffusion resistance of electrolyte; (2) provide ideal electron pathway even in a very rapid charge/discharge reaction; and (3) load more active materials per unit electrode area due to its high surface area.

The 3D hybrid electrode material was prepared by a simple two-step hydrothermal process, which can easily scale up. First, the CoO nanowires were synthesized on nickel foam by a hydrothermal process as described previously.[25] In detail, 0.582 g $Co(NO_3)_2$ and 0.6 g urea were dissolved in 50 mL deionized water, the obtained homogeneous solution was further transferred into Teflon-lined stainless steel autoclave with a piece of clean nickel foam ($10 \times 15 \times 0.1$ $mm^3$, 100 PPI, 330 g $m^{-2}$, Changsha Lyrun Material Co., Ltd. China) immersed into the reaction solution. After 8 h growth at 95 °C, the as-prepared precursors were annealed under a constant flow of argon (50 sccm) at 450 °C for 2 h; Then the nickel foam with CoO nanowires was immersed into a 0.1 M $Ni(NO_3)_2$ aqueous solution and maintaining at 85 °C for 5 h. After cooling to room temperature, the samples were obtained.

Samples were characterized by scanning electron microscopy (SEM) (JSM-6700F, 10.0 kV), transmission electron microscopy (TEM) (JEM-2010FEF, 200 kV) equipped with an energy dispersive X-ray spectrometry (EDS), powder X-ray diffraction (XRD) (Bruker D-8 Avance) measurement, and Fourier transform infrared (FTIR) spectrum was recorded on a Bruker Vertex 80V HYPERION 2000 Microscope using MCT detector. The mass of electrode materials was measured on an AX/MX/UMX Balance (METTLER TOLEDO, maximum = 5.1 g; $d = 0.001$ mg).

Electrochemical measurements (ZAHNER ZENNIUM Electrochemical Workstation) were performed in a three-electrode electrochemical cell at room temperature using a 1 M NaOH as electrolyte. The nickel foam supported hybrid nanostructure (~1 $cm^2$ area; CoO mass: ~2.2 mg; NiHON mass: ~0.8 mg) acted directly as the working electrode. A Pt plate and Ag/AgCl were used as the counter electrode and the reference electrode, respectively. All potentials were referred to the reference electrode. The weight in specific capacitance (F $g^{-1}$) and current rate (A $g^{-1}$) was calculated based on the whole mass of the two active materials (CoO and NiHON). Electrochemical impedance spectroscopy (EIS) measurements were carried out by applying an AC voltage with 1 mV amplitude in a frequency range from 0.1 Hz to 100 kHz at open circuit potential.

The SEM image in Fig. 1a shows that nickel foam has a 3D porous structure. Fig. 1b indicates the aligned CoO nanowires are ~60–100 nm and ~2–3 μm in diameter and length, respectively, and the magnified image in the inset reveals they are highly porous. This result corresponds well with previous report where porous but single-crystalline CoO naowires were directly grown on titanium foil.[25] Fig. 1c, d show the hybrid structure on the nickel foam. A typical image of a part of nickel foam, as shown in Fig. 1c, indicates that after growth the nickel foam is uniformly covered with the hybrid structure. From Fig. 1d, it is clearly observed that the CoO

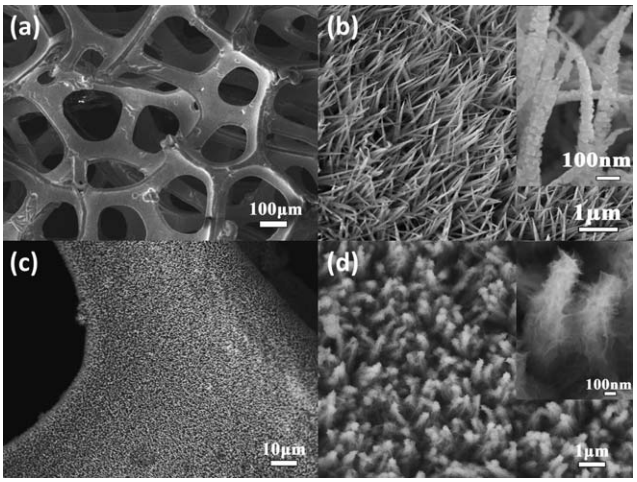


**Fig. 1** SEM images of (a) the 3 D structure of nickel foam, (b) the CoO nanowire on the nickel foam. (c,d) low and high magnification images of the hybrid structure on the nickel foam. Insets in Fig. 1b and 1d are the enlarged pictures.

"nanostems" are tightly bonded and totally covered with "leaves" of nanoflakes, so the space between the CoO arrays is abundantly utilized, which would increase the energy and power per unit area. The nanoflakes are formed because of $Ni^{2+}$ hydrolysis on the CoO surface,[26] which leads to the hydrotalcite-like nickel hydroxide structure intercalated with the $NO_3^-$ group. The hierarchical hybrid structure is further illustrated from the TEM image in Fig. 2. As can be seen in Fig. 2a, the surface of CoO nanowire is fully covered with ultrathin nanoflakes, which stretch out about 100 nm. EDS analysis in two typical areas (A1, A2) reveals the elements of O, N and Ni in the "leaves".

The XRD patterns of the CoO nanowires and the hybrid nanostructure are shown in Fig. 3a. The CoO nanowires corresponds with the reported pattern of CoO (JCPDS, card no: 48-1719). After the second step growth, other two peaks appear in the XRD pattern of the hybrid structure, which correlate with previous report of $Ni_3(NO_3)_2(OH)_4$ (JCPDS, card no: 22-0752).[27] The FTIR spectrum

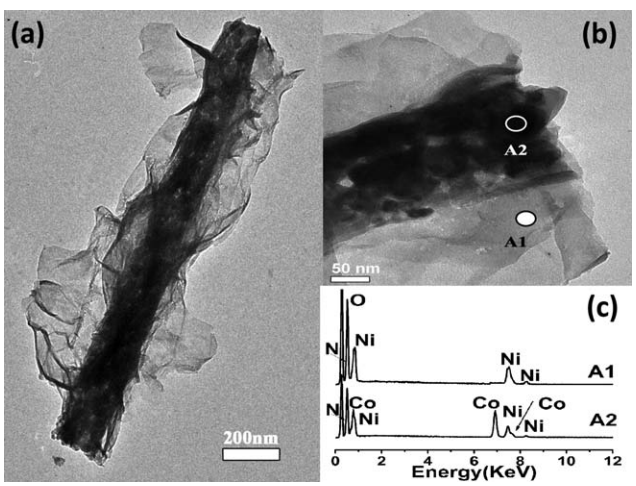


**Fig. 2** TEM images of an individual hybrid nanostructure. The EDS signals of the areas labeled as A1 and A2 in (b) are shown in (c).

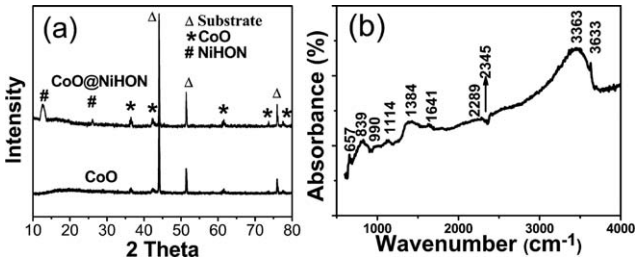


**Fig. 3** (a) XRD patterns of the CoO nanowire and the hybrid structure on the nickel foam. (b) FTIR spectrum of the hybrid structure.

in Fig. 3b provides further evidence for the formation of Ni-based hydroxidenitrate. In detail, a group of peaks in the range of 990 to 1384 $cm^{-1}$ represent the nitrate anion.[28] Two peaks observed at 657 and 3633 $cm^{-1}$ are associated with the σ–OH vibrations and ν–OH stretching, respectively.[29] Three peaks at 839, 1641, and 3363 $cm^{-1}$ are associated with the vibrations of $H_2O$.[30]

Fig. 4a shows the cyclic voltammetry (CV) curves of the hybrid structure on nickel foam at different scan rates of 5, 10, 20, 40, and 80 mV $s^{-1}$. To better understand the reaction, the CV property of CoO nanowires on nickel foam (nanostructures obtained after step 1 in experiment section) at 40 mV $s^{-1}$ is also shown as the dotted curve in Fig. 4b, from which two pairs of redox peaks can be observed:

P1 and P3 are due to the reaction,[31]

$$CoO + OH^- \leftrightarrow CoOOH + e^-$$

P2 and P4 are due to the reaction:

$$CoOOH + OH^- \leftrightarrow CoO_2 + H_2O + e^-$$

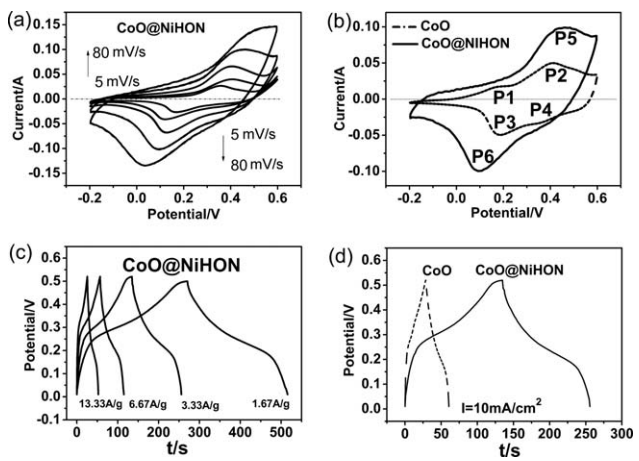


**Fig. 4** (a) The CV curves of the hybrid structure on nickel foam at different scan rates of 5, 10, 20, 40 and 80 mV $s^{-1}$, (b) Comparison of the hybrid structure and CoO nanowires on nickel foam at the same scan rate of 40 mV $s^{-1}$. (c) Charge–discharge behavior of the hybrid structure on nickel foam at different current densities. (d) The comparison of the hybrid structure and CoO nanowires on nickel foam with the same areal charge–discharge current of 10 mA $cm^{-2}$. Note that the redox peaks due to the Ni foam are negligible as shown in the Electronic Supplementary Information (Fig. S1†).

Comparing it with the solid curve in Fig. 4b, which is the CV curve of the hybrid structure on nickel foam at the same scan rate (40 mV $s^{-1}$), the great contribution of ultrathin NiHON nanoflake can be confirmed. The CV curve of the hybrid structure has not only fully encompassed all the four peaks of the CoO nanowires, but greatly expanded, thus increasing the integrated area, which means the hybrid structure has a much larger capacitance than only the CoO nanowires. On account of NiHON nanoflake, the expanded peaks (P5 and P6) are mainly attributed to the reaction between $Ni^{2+}/Ni^{3+}$ and anions $OH^-$.[32] So the ultrathin NiHON nanoflake did not restrain the inside CoO nanowire from reaction with $OH^-$, but introduces another electrochemical redox reaction to boost the charge storage capability.

This conclusion is further confirmed by charge–discharge testing. Fig. 4c shows the charge–discharge behavior of the hybrid structure between 0.01–0.52 V at different current densities. The SC is calculated as follows:

$$C = It/m\Delta V \quad (1)$$

Where $I$ is the discharge current, $m$ is the mass of the hybrid structure, $\Delta V$ is the potential window, $t$ is the discharge time, and $C$ is the specific capacitance. A nickel foam under the same pretreatment was also tested independently, which shows a capacitance of only ~2 F $g^{-1}$ at a current density of 5 mA $cm^{-2}$, contributing only 2.89% of the total capacitance of the hybrid structure (calculation details are in the Electronic Supplementary Information, ESI†). In order to illustrate the contribution from the active material, in all of the following results the small contribution of the Ni foam was subtracted. From formula (1), the hybrid structure has SCs of 671.3, 749.9, 781.8 and 798.3 F $g^{-1}$ at different discharge currents of 13.33, 6.67, 3.33 and 1.67 A $g^{-1}$, respectively. Fig. 4d shows the comparison of the hybrid structure and CoO nanowires on nickel foam with the same areal charge–discharge current of 10 mA $cm^{-2}$. In short, because of the participation of NiHON, the hybrid structure exhibits much better electrochemical performance when compared with CoO nanowires alone (which has a SC of 307 F $g^{-1}$ at a current density of 4.55 A $g^{-1}$). Furthermore, if the CoO and NiHON could be simply added together with the same mass ratio to that in the hybrid structure, the SC of this addition would be only ~545 F $g^{-1}$ (calculation details are in the ESI†). This evidence further shows the merits of the uniformly hybrid structure which has almost single-crystalline backbones and ultrathin nanoflake shells.

The electrochemical stability of CoO nanowires and the hybrid structure are shown in Fig. 5a. After 2000 cycles of charge and discharge, both materials did not show evident loss of capacitance (less than 5%), and the hybrid structure with a 96.7% capacitance retention showed even better durability than the CoO nanowires alone (which has a 95.1% capacitance retention). Fig. 5b shows the last 10 charge–discharge cycles of the hybrid structure. After long-time cycling, the hybrid structure still maintains a good electrochemical reversibility with 98.9% Coulombic efficiency. The good electrochemical stability can be explained in two parts: First, the ordered CoO nanowires have grown tightly on nickel foam and provide an excellent conducting connection with the NiHON nanoflake; Second, the NiHON nanoflake, filled in the surface of CoO nanowires, can prevent the 'stem' from collapsing during the harsh long-duration reaction in the electrolyte.[33] Fig. 5c further reveals the current density dependence of the cycling performance. During the

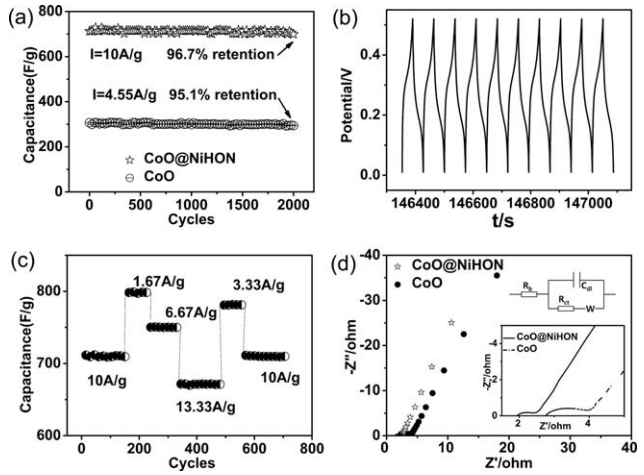


**Fig. 5** (a) Cycling performance of the hybrid structure and CoO nanowires. (b) Last 10 charge–discharge curves of the hybrid structure. (c) The current density dependence of the hybrid structure. (d) Impedance Nyquist plots of the hybrid structure and CoO nanowires on nickel foam at open circuit potential.

the first 150 cycles with a charge–discharge density of 10 A $g^{-1}$, the hybrid structure shows a stable SC of ~710 F $g^{-1}$. In the following 400 cycles, although the charge–discharge rate changes successively, the hybrid structure always demonstrates stable capacitance in each situation. When the current turns back to 10 A $g^{-1}$, a fully recovered SC of ~710 F $g^{-1}$ is observed in the following 150 cycles, which demonstrates the hybrid structure has excellent rate capability.

Electrochemical impedance spectroscopies (EIS) of the two structures are shown in Fig. 5d, with a well-fitted equivalent circuit showing the components of the whole impedance. In low frequency area, the slope of the curve shows the Warburg impedance ($W$) which represents the electrolyte diffusion in the porous electrode and proton diffusion in host materials. CoO @ NiHON on nickel foam has the more ideal straight line along the imaginary axis, which demonstrates it has lower diffusion resistance.[34] This can be attributed to the ultrathin NiHON nanoflake with large surface area that has enhanced the electrode materials utilization and thus facilitates the supply of $OH^-$ to the entrance of CoO nanopores and nickel foam micropores.[35] In the high frequency area, the intersection of the curve at real part $Z'$ (which is equal to $R_b$) indicates the bulk resistance of the electrochemical system, and the semicircle (which corresponds to double layer capacitance $C_{dl}$ and charge-transfer resistance $R_{ct}$) displays the charge-transfer process at the working electrode–electrolyte interface.[36] From the inset picture in Fig. 5d, the hybrid structure also displays lower bulk resistance and charge-transfer resistance than CoO nanowires. It is believed that the combination of low diffusion and electron-transfer resistances are responsible for the excellent electrochemical performance of the hybrid structure.

In summary, a novel hybrid nanostructure with two active materials (ultrathin NiHON nanoflake and CoO nanowire) has been fabricated on the 3D nickel foam substrate. Detailed electrochemical characterization shows the hybrid structure has combined the merits of the two active components, and it has an excellent electrochemical stability, high rate performance and a maximum specific capacitance of 798.3 F $g^{-1}$. The cost-effective fabrication and excellent electrochemical performance provide great potential for this type of hybrid 3D nanostructure as an active electrode for electrochemical supercapacitors.

## Acknowledgements

H.Z. thanks the support from the CREATE program (Nano-materials for Energy and Water Management) from NRF in Singapore.

## References

1 J. R. Miller and P. Simon, *Science*, 2008, **321**, 651.
2 P. Simon and Y. Gogotsi, *Nat. Mater.*, 2008, **7**, 845.
3 R. Kötz and M. Carlen, *Electrochim. Acta*, 2000, **45**, 2483.
4 S. J. Guo and S. J. Dong, *Chem. Soc. Rev.*, 2011, **40**, 2644.
5 T. Cottineau, M. Toupin, T. Delahaye, T. Brousse and D. Bélanger, *Appl. Phys. A: Mater. Sci. Process.*, 2005, **82**, 599.
6 L. Li, T. Y. Zhai, H. B. Zeng, X. S. Fang, Y. Bando and D. Golberg, *J. Mater. Chem.*, 2011, **21**, 40.
7 M. D. Stoller and R. S. Ruoff, *Energy Environ. Sci.*, 2010, **3**, 1294.
8 G. Lota, K. Fic and E. Frackowiak, *Energy Environ. Sci.*, 2011, **4**, 1592.
9 C. C. Hu, K. H. Chang, M. C. Lin and Y. T. Wu, *Nano Lett.*, 2006, **6**, 2690.
10 M. Toupin, T. Brousse and D. Bélanger, *Chem. Mater.*, 2002, **14**, 3946.
11 S. L. Xiong, C. Z. Yuan, X. G. Zhang, B. J. Xi and Y. T. Qian, *Chem.–Eur. J.*, 2009, **15**, 5320.
12 Y. G. Li, B. Tan and Y. Y. Wu, *Nano Lett.*, 2008, **8**, 265.
13 K. W. Chung, K. B. Kim, S. H. Han and H. K. Lee, *Electrochem. Solid-State Lett.*, 2005, **8**(5), A259.
14 M. Toupin, T. Brousse and D. Bélanger, *Chem. Mater.*, 2004, **16**, 3184.
15 S. Chen, J. W. Zhu, X. D. Wu, Q. F. Han and X. Wang, *ACS Nano*, 2010, **4**(5), 2822.
16 S. Chen, J. W. Zhu and X. Wang, *J. Phys. Chem. C*, 2010, **114**, 11829.
17 J. Jiang, Y. Y. Li, J. P. Liu and X. T. Huang, *Nanoscale*, 2011, **3**, 45.
18 R. Liu and S. B. Lee, *J. Am. Chem. Soc.*, 2008, **130**, 2942.
19 G. Y. Zhao, C. L. Xu and H. L. Li, *J. Power Sources*, 2007, **163**, 1132.
20 H. G. Zhang, X. D. Yu and P. V. Braun, *Nat. Nanotechnol.*, 2011, **6**, 277.
21 L. H. Bao, J. F. Zang and X. D. Li, *Nano Lett.*, 2011, **11**, 1215.
22 G. R. Li, Z. L. Wang, F. L. Zheng, Y. N. Ou and Y. X. Tong, *J. Mater. Chem.*, 2011, **21**, 4217.
23 Y. Yu, G. B. Ji, J. M. Cao, J. S. Liu and M. B. Zheng, *J. Alloys Compd.*, 2009, **471**, 268.
24 Y. B. He, G. R. Li, Z. L. Wang, C. Y. Su and Y. X. Tong, *Energy Environ. Sci.*, 2011, **4**, 1288.
25 J. Jiang, J. P. Liu, R. M. Ding, X. X. Ji, Y. Y. Hu, X. Li, A. Z. Hu, F. Wu, Z. H. Zhu and X. T. Huang, *J. Phys. Chem. C*, 2010, **114**, 929.
26 J. P. Liu, Y. Y. Li, H. J. Fan, Z. H. Zhu, J. Jiang, R. M. Ding, Y. Y. Hu and X. T. Huang, *Chem. Mater.*, 2010, **22**, 212.
27 J. P. Liu, C. W. Cheng, W. W. Zhou, H. X. Li and H. J. Fan, *Chem. Commun.*, 2011, **47**, 3436.
28 K. Vivekanandan, S. Selvasekarapandian and P. Kolandaivel, *Mater. Chem. Phys.*, 1995, **39**, 284.
29 N. A. M. Barakat, M. S. Khil, F. A. Sheikh and H. Y. Kim, *J. Phys. Chem. C*, 2008, **112**, 12225.
30 B. Pejova, A. Isahi, M. Najdoski and I. Grozdanov, *Mater. Res. Bull.*, 2001, **36**, 161.
31 L. Cao, F. Xu, Y. Y. Liang and H. L. Lin, *Adv. Mater.*, 2004, **16**, 1853.
32 C. Y. Cao, W. Guo, Z. M. Cui, W. G. Song and W. Cai, *J. Mater. Chem.*, 2011, **21**, 3204.
33 J. P. Liu, J. Jiang, C. W. Cheng, H. X. Li, J. X. Zhang, H. Gong and H. J. Fan, *Adv. Mater.*, 2011, **23**, 2076.
34 K. P. Wang and H. S. Teng, *J. Electrochem. Soc.*, 2007, **154**, A993.
35 M. W. Xu, L. B. Kong, W. J. Zhou and H. L. Li, *J. Phys. Chem. C*, 2007, **111**, 19141.
36 C. W. Huang and H. Teng, *J. Electrochem. Soc.*, 2008, **155**, A739.